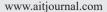


European Journal of Remote Sensing

An official journal of the Italian Society of Remote Sensing





Relative importance analysis of Landsat, waveform LIDAR and PALSAR inputs for deciduous biomass estimation

Alyssa Endres¹, Giorgos Mountrakis^{1*}, Huiran Jin², Wei Zhuang¹, Ioannis Manakos³, John J. Wiley Jr⁴ and Colin M. Beier⁵

¹Department of Environmental Resources Engineering, State University of New York
College of Environmental Science and Forestry, Syracuse, NY 13210, USA

²Department of Geographical Sciences, University of Maryland, College Park, MD 20742, USA

³Information Technologies Institute, Centre for Research and Technology Hellas, Thessaloniki, Greece

⁴Department of Environmental and Forest Biology, State University of New York
College of Environmental Science and Forestry, Syracuse, NY 13210, USA

⁵Department of Forest and Natural Resources Management, State University of New York
College of Environmental Science and Forestry, Syracuse, NY 13210, USA

*Corresponding author, e-mail address: gmountrakis@esf.edu

Abstract

Aboveground forest biomass estimation is an integral component for climate change, carbon stocks assessment, biodiversity and forest health. LiDAR (Light Detection And Ranging), specifically NASA's Laser Vegetation Imaging Sensor (LVIS), PALSAR (Phased Array type L-band Synthetic Aperture Radar), and Landsat data have been previously used in biomass estimation with promising results when used individually. In this manuscript all three products are jointly utilized for the first time to assess their importance for deciduous biomass estimation. Results indicate that LVIS inputs are ranked as most important followed by PALSAR inputs. Particularly for PALSAR, scenes acquired in May and August were ranked higher compared to other months.

Keywords: Biomass estimation, remote sensing, optical; radar, Lidar, fusion.

Introduction

Forest aboveground biomass estimations play an important role in numerous environmental studies and are at the core of important policy making. Examples include assessment of carbon stocks for policies and initiatives, bioenergy production, mapping and planning fuel treatments, and for developing sustainable forest and wildlife management strategies. Collecting accurate ground-based estimations requires a dense network of inventory plots, high associated costs, and significant man power. By using remote sensing as an alternative, forest aboveground biomass (referred as biomass) estimation becomes more feasible and practical when trying to cover large areas. However, there are several data sources, statistical methods, and prediction standards for doing so and there is a disagreement on



which practices are best for the task [Fassnacht et al., 2014]. A recent survey of aboveground biomass estimation methods in forest ecosystems using remotely sensed data in available in [Lu et al., 2014].

Optical sensors like the Landsat series produce readily available time-series data sets, so data from the Landsat Thematic Mapper (TM) and Landsat Enhanced Thematic Mapper Plus (ETM+) are commonly used to estimate biomass [Phua and Saito, 2003; Lu, 2005]. Random forest algorithms and multiple linear regression techniques were used for biomass predictions. On large scales, Landsat ETM+ images produced detailed and accurate biomass estimations. The most accurate estimations result from including land cover information on vegetation phenology [Avitabile et al., 2012]. Dube and Mutanga [2015] also provide evidence for the strength and potential of using data from the multispectral Landsat 8 Operational Land Imagery. They tested different sets of spectral analysis including the spectral bands, spectral vegetation indices, and the combination of the two. They compared the results of Landsat 8 with estimations using Landsat 7 ETM + and concluded that the more recent Landsat 8 data produced higher estimation accuracies. Hyperspectral data has also been used for biomass estimation (for example [Filippi et al., 2014]). A major limitation for accurate remotely sensed biomass estimation is caused by the fact that typical optical remote sensors only capture the signals from the surface of the forest canopy.

Due to radar's ability to collect information independent of weather conditions, synthetic aperture radar (SAR) data is valuable for forest biomass mapping [Dobson et al., 1992; Ranson and Sun, 1994; Rignot et al., 1997; Santoro et al., 2002a, 2002b; Thiel et al., 2006]. Winter coherence data and summer intensity values of the L-band ALOS/PALSAR data were successfully used to examine the mapping of different forest areas. Two-date (wet and dry season) dual polarization (HH and HV) synthetic aperture radar imagery was used to evaluate biomass estimations, whereas the inputs used included different types of texture processing and various combinations of single and dual polarization ratios. The L-band dual polarization SAR data produced valuable results and it demonstrated that there is potential for using PALSAR data for biomass estimations, improving biomass estimations when compared to older data from JERS-1 [Sarker et al., 2012].

Regression modelling can determine the relation between biomass derived from in-situ data and ALOS/PALSAR data [Carreiras et al., 2012]. Various regression models were evaluated to determine the relationship between forest biomass derived from field measurements and ALOS/PALSAR backscatter in Peregon and Yamagata [2013]. Most reliable biomass estimations were obtained using the ALSOS/PALSAR HV-polarized backscatter with the Water Cloud model. The work in Morel et al. [2011] integrated field data with ALOS PALSAR imagery to both discriminate oil palm plantations from forest stands, and predict AGB (above ground biomass) using logarithmic regression analysis of HV-polarized PALSAR data. Regression analysis was also used in Hamdan et al. [2011] to identify the relationship between ALOS PALSAR backscatter and AGB in tropical forests, while a logarithmic regression curve, which strongly correlates the ALOS/PALSAR backscatter intensity and the boreal forest AGB, was estimated in Suzuki et al. [2013]. A machine learning algorithm (based on bagging stochastic gradient boosting) to correlate AGB estimated from field data and ALOS PALSAR was employed in Carreiras et al. [2012] to retrieve the AGB of woody vegetation in West Africa. Moreover, an empirical function was estimated correlating the AGB measured on the ground sample plots with several image variables derived from L-band ALOS/PALSAR polarizations in Hamdan et al. [2014]. A common conclusion in Deng et al. [2014], Attarchi and Gloaguen [2014], Mitchard et al. [2012], Koch [2010], Hyyppä et al. [2009] is that there is stronger relationship between AGB and ALOS/PALSAR data in the HV rather than the HH polarization mode.

Except for methods that rely on remote sensing data coming only from ALOS PALSAR imagery to estimate biomass, there are several approaches combining ALOS PALSAR imagery with other types of remote sensing data. The study in Deng et al. [2014] used principal component analysis and multivariate linear regression for combining variables extracted from ALOS/PALSAR and WorldView-2 data in order to improve the accuracy of biomass estimation in highly dense forests. Additionally, an approach based on multiple linear regressions [Attarchi and Gloaguen, 2014] was used to jointly use Landsat ETM+ and ALOS/PALSAR data for the AGB estimation in mountainous and high biomass forests. Proceeding a step further, the method in Mitchard et al. [2012] proposed a processing chain that combines ALOS PALSAR, space borne LiDAR and ground-based data for mapping tropical forest biomass, overcoming problems of saturation at higher biomass values and persistent cloud coverage.

In order to obtain accurate estimations, information on the vertical forest structure is needed, since biomass is closely related to both the size and spatial distribution of trees. Since LiDAR data can provide detailed vertical information they demonstrate significant advantages for biomass estimation. Koch [2010] discusses various approaches. Mallet and Bretar [2009], Hyyppä et al. [2009], Chang et al. [2015], Dees and Koch [2008] show that high quality information related to height and forest structure information can be extracted from the imagery. Su et al. [2016] demonstrate the effectiveness of ground inventory, Geoscience Laser Altimeter System (GLAS)/Ice, Cloud, and Land Elevation Satellite (ICESat) data, optical imagery, climate surfaces, and topographic data to estimate aboveground biomass in China. Hayashi et al. [2015] used ICESat and GLAS satellite LiDAR data to demonstrate the importance of using LiDAR data for the monitoring of forest resources. Estimating forest aboveground biomass using data from NASA's Land, Vegetation, and Ice Sensor (LVIS) is also available. This was shown by Huang et al. [2013], Sun et al. [2011] while using radar synergies. Zhuang et al. [2015] developed and evaluated a set of Gaussian Decomposition metrics. By explicitly incorporating both LiDAR intensity and vertical structures of the canopy layers the biomass estimation accuracy increased. LVIS data have been also successfully implemented for accurate ground detection by ground peak identification [Zhuang and Mountrakis, 2014a], extracting tree heights [Zhuang and Mountrakis, 2014b] and calculating Leaf Area Index (LAI) values [Tang et al., 2014].

For reliable biomass estimations having accurate tree and forest type, crown coverage, forest layer structure, and height data is critical. In addition to this important but diverse biophysical information, different frame conditions, saturation, weather limitations are imposed on datasets so that no single data type can fulfil all requirements needed to directly derive biomass from remote sensing data. This has led to a collection of biomass estimation approaches where information is fused from multiple sensors. Koch [2010] provides evidence in support of using advanced remote sensing techniques and new data including full wave laser scanning data, polarimetric radar interferometry, and hyperspectral data to assess forest biomass. Lu [2006] evaluates the potential of combining spectral responses and image textures to improve estimations. By fusing LiDAR and optical data sets, estimations

for wood volume and biomass can be improved as shown Straub et al. [2009], Dees et al. [2006], Maltamo et al. [2006]. Moghaddam et al. [2002] were able to achieve better results when they combined AirSAR and Landsat TM data sets compared to using a single data set. Banskota et al. [2009] found that, on their own, neither imaging LiDAR nor BioSAR (a radar system designed to aid in the estimation of biomass) were reliable predictors for biomass, but combined achieved a successful result. Fassnacht et al. [2014] conducted a literature review and two case studies in Germany and Chile with LiDAR and airborne hyperspectral data. It was determined that the sensor type is the most important factor in obtaining accurate biomass estimates, with LiDAR data being preferable to hyperspectral data. The prediction method also had a considerable effect on the accuracy, in which the random forest performed the best. A large number of reference sample points on the ground resulted in the lowest error for biomass predictions [Fassnacht et al., 2014]. Swatantran et al. [2011] estimated biomass in the Sierra Nevada using a fusion of structural metrics from the Laser Vegetation Imaging Sensor (LVIS) and spectral characteristics from the Airborne Visible Infrared Imaging Spectrometer (AVIRIS). They established that the LVIS variables were consistently good predictors of both total and species specific biomass. LiDAR is better for biomass estimation, but hyperspectral data can be used to refine the predictions through a priori species stratification [Swatantran et al., 2011]. It is concluded that using a combination of sensors has benefits in various applications.

One major limitation of current research is the lack of integration of three multi-date sensors for biomass estimation. Accordingly, in this manuscript we investigate fusion of optical, LiDAR and radar sensors for biomass estimation. More specifically, we examine individual sensor performance, multi-date performance and multi-sensor integration of three popular sensors, namely the optical Landsat, the waveform LiDAR LVIS and radar PALSAR sensors. We concentrate on variable ranking instead of model fitting performance to provide general guidance on the inputs that users can later implement in their own study areas.

Materials and Methods

The Central New York State, primarily within Onondaga County, comprises the study area. The study contains deciduous stands that vary in ages from 20 to 100 or more years. Our study did not include any coniferous stands. There is a variety of deciduous species present within the stands [Zhuang et al., 2015]. Three sensors are examined, Landsat, LVIS, PALSAR to incorporate optical, LiDAR and Radar information, respectively.

Optical

Landsat is the first choice due to its wide and consistent spatial coverage, and the extensive familiarity of the remote sensing community. Landsat data included leaf-on and leaf-off information from July 15, 2009 and April 10, 2009, respectively. The data includes the top of atmosphere reflectance in bands 1, 2, 3, 4, 5, and 7 for both scenes. The Normalized Difference Vegetation Index (NDVI) was calculated from bands 3 and 4. Standard deviations were also calculated with a 3x3 window for each of the six bands and for the NDVI. In total, 14 inputs were tested for each image.

Radar

Phased Array type L-band Synthetic Aperture Radar (PALSAR) is an important alternative to optical remote sensing because of its active microwave sensing system which allows it to acquire images whether it is day or night and regardless of the weather. The PALSAR data included intensity, polarimetry, interferometry, and texture information from four scenes in the Fine Beam Dual (FBD) polarization mode with HH and HV polarizations from May 12, June 27, August 12, and November 12, 2010. All images were acquired in an ascending orbit (path 134, frame 850) and an off-nadir angle of 34.3 degrees. Pixel spacing is 9.37 m in the slant range direction, and 3.17-3.20 m in the azimuth direction. Intensity data consisted of both HH and HV backscattering coefficients (σ0), the difference between the two and the ratio between the polarization bands (Tab. 1). The interferometric coherence was calculated for each polarization band for every combination of dates. Texture measures included energy (ENE), contrast (CON), dissimilarity (DIS), homogeneity (HOM), entropy (ENT), and correlation (COR). To keep the size of textural feature space manageable, only two window sizes were tested, one at a smaller scale of 90 m (i.e. 3 pixels) and the other at a larger scale of 450 m (i.e. 15 pixels). The total number of PALSAR-derived inputs was 132.

Table 1 - Summary of features that were extracted from the PALSAR FBD data (adapted [Jin et al., 2014]). Explanations for the abbreviations are cited in the text.

Category	Variable	Data					Number of layers	
Intensity	$egin{array}{c} \sigma_{ m HH}^0 \ & \sigma_{ m HV}^0 \ & \sigma_{ m HH}^0 - \sigma_{ m HV}^0 \ & \sigma_{ m HH}^0 / \sigma_{ m HV}^0 \end{array}$	May12,	16 (4×4)					
Polarimetry ¹	Н <i>а</i>	May12, Jun27, Aug12, Nov12						8 (2×4)
Interferometry	$\gamma_{ m HH}$ $\gamma_{ m HV}$	Image pair			Δ t (days)	B 2(m)	B⊥³(m)	
		May12	vs.	Jun27	46	220	158	
		May12	vs.	Aug12	92	493	641	12 (2×6)
		May12	vs.	Nov12	184	381	529	
		Jun27	vs.	Aug12	46	273	484	
		Jun27	vs.	Nov12	138	161	371	
		Aug12	vs.	Nov12	92	112	113	
Texture	ENE							
	CON		05 (2) (4) (4) (2)					
	DIS	$\sigma_{ m HH}^0, \sigma_{ m H}^0$						
	HOM	on May 1		96 (2×4×4×2)				
	ENT							
	COR							

 1 Polarimetric parameters H and α were derived based on dual-polarized data. 2 Parallel baseline. 3 Perpendicular baseline. * Two window sizes were used for texture computation.

LiDAR

The large footprint LiDAR sensors have shown high potential towards detecting the vertical structural complexity of forests thus adding important information to conventional multispectral remote sensors. Our LiDAR sensor was the Laser Vegetation Imaging Sensor (LVIS), a full waveform LiDAR sensor that NASA is planning to install on the International Space Station at the Global Ecosystem Dynamics Investigation (GEDI). LiDAR waveform data was collected from the August 24-26, 2009 with the leaves fully on the trees. The LVIS circular pulse was operating at a wavelength of 1064 nm. The footprint diameter is nominally 20 m on the ground. The vertical resolution of the waveform data was approximately 0.3 m. Scanning angle varied from 0 to 5 degrees. Within each waveform, a total of 432 time bins were recorded [Zhuang and Mountrakis, 2014a]. From the data, 13 metrics were calculated based on Gaussian decomposition (GD) and 12 non-GD metrics were based on height and statistics analysis. Further information on the LVIS inputs is provided in Zhuang et al. [2015].

Reference data

Field measurements (DBH, species, and crown height) were taken from July to September 2011 in 10 meter radius plots to serve as a reference for biomass estimations. Details on the field biomass estimation are provided in Zhuang et al. [2015]. In total there were 24 deciduous plots that overlapped with data from all three sensors. While a higher number of plots would have been desirable, this limited number is still deemed sufficient to show us general patterns. Furthermore, we fully trust the field measurements as we were part of the collecting team.

Regression model

We chose the random forest technique as our regression method due to its ability to rank the importance of all input variables [Liaw and Wiener, 2002]. Initial parameters included one hundred trees, learning rates between 0.1 and 1 using a step size of 0.1, and maximum number of splits between one and eight. The algorithm selected the best values for learning rate and number of splits based on a leave-one-out cross validation and the lowest mean squared error. In total there were 185 inputs for the random forest regression algorithm between the three sensor datasets. Liaw and Wiener's random forests for regression with cross validation (a Matlab port available for download from https://code.google.com/p/randomforest-matlab/) was used to perform all calculations.

Results and Discussion

The random forest algorithm with cross-validation resulted in a final forest with 50 trees, a maximum number of splits of one, and had a learning rate of 0.056. The relative importance values from the algorithm for deciduous plots are shown in Table 2 when all sensor inputs were used. Of the 185 variables, the algorithm returned 28 inputs for deciduous plots that had a relative importance greater than 5% when compared to the most important variable. Of those inputs, ten of the variables were from LVIS, 16 were from single time observations from PALSAR, and two were derived from bi-temporal PALSAR images. Of the ten LVIS inputs, four were from Gaussian Area Index (GAI) metrics, where GAI is the area covered by a Gaussian function and two were from Gaussian Decomposition (GD) metrics. The

other four were from non-GD metrics. The most important input from Landsat was the standard deviation of band 7 of the April image using a 3x3 window and had an importance of 1.08% compared to the most important input.

The LVIS and PALSAR sensors have the ability to obtain more information than Landsat regarding the forest structure. For the deciduous plots, the inputs proposed by Zhuang et al. [2015], including the new GAI and existing GD metrics, were most important inputs. The RatioE (normalized GAIEHSum) was most important followed by the GAIEHSum, RH100, MeanHeight, and FirstCentroid. These five inputs relate to the height. The two important multi-temporal PALSAR variables were the interferometric coherence with HH backscattering coefficients between May and August and between June and August. These inputs had a higher relative importance than most of the texture variables from single-time PALSAR data from individual months (May, June, August, and November). With greater information about the height of forests, more accurate estimations can be produced, since most optical sensors only capture the surface reflection of the canopy. The top three inputs, RatioE, GAIEHSum, and RH100 are almost twice as important as the next most important variables. The importance of the selected GD metrics shows that, in addition to the heights the intensity information of different canopy layers characterized by the extracted Gaussian components, contributes significantly to biomass estimation.

Overall, features extracted from PALSAR and LVIS are more important than Landsat features in biomass estimation. This is because in forested areas biomass is largely determined by the amount of branches and leaves of the tree canopy. A tree with multiple canopy layers is expected to have a higher biomass value compared to a tree with a single canopy layer. Dense canopy (i.e. more complex canopy structure) usually leads to a higher possibility of the radar and LiDAR signals being returned and detected by the sensor. If the signal hits a tree with only one layer of leaves, more likely the signal will bounce away from the sensor direction. Therefore, the intensity of the returned signals detected by active sensors is indicative of forest canopy structure, and of more importance in biomass estimation. In contrast, Landsat-derived variables are less effective because what Landsat receives is the reflected sunlight at the top of the tree. Whether a tree has a single- or multi-layer canopy makes little difference in spectrum of tree cover.

While this work uses a limited number of plots for which information from LiDAR, PALSAR, and Landsat were available, the results from this research showcase the importance of LiDAR and radar datasets for biomass estimation. Considering the upcoming satellite missions of ICESat II and GEDI exciting new biomass monitoring opportunities exist. European radar sensors are already operative (e.g. Sentinel-1a and -1b satellites) and following a free distribution policy there is potential, especially utilizing the vast amount of C-band data. However, possibility for improvement remains low, since the penetration degree, especially in dense forest canopies is limited. On the other hand, higher expectations are placed on the recently announced Airbus DS UK Biomass satellite able to capture information on P-band and account for the European Space Agency's forest-carbon monitoring requirements (from 2021 and on). Furthermore, combinations of C- and P-band data are going to further advance the level of accuracy, since information for both canopy surface and structure may be more efficiently acquired. To that end we expect that this work may pave the way for researchers and be enhanced through current and upcoming missions.

 $Table\ 2\ (Continued\ on\ the\ next\ page)\ -\ Variable\ relative\ importance\ for\ deciduous\ plots.$

Input Abbreviation	Definition	Importance
RatioE	LVIS Normalized GAIEHSum by an exponentially transformed mean height	1.00
GAIEHSum	LVIS Summation of canopy GAI above ground height-weighted by exponentially transformed mean height	1.00
RH100	LVIS Relative height; above ground height at which 100% of the waveform energy occurs	0.96
MeanHeight	LVIS Mean height above the ground of all the Gaussian centroids	0.63
FirstCentroid	LVIS Aboveground height of the highest Gaussian centroid	0.63
Ratio	LVIS Normalized GAIHSum (Summation of canopy GAIs, each weighted by the height of its centroid)	0.63
GAIHSum	LVIS Summation of canopy GAIs, each weighted by the height of its centroid	0.56
γ_HH (Aug vs. May)	PALSAR Interferometric coherence between August and May with HH backscattering coefficient	0.47
Tex_May_ENT_HV_Win3	PALSAR Texture measure entropy extracted from May HV back- scattering with a window size of 3x3	0.44
Tex_Aug_ENE_HH_Win3	PALSAR Texture measure energy extracted from August HH back- scattering with a window size of 3x3	0.44
γ_HH (Aug vs. Jun)	PALSAR Interferometric coherence between August and June with HH backscattering coefficient	0.38
Tex_May_ENE_HV_win3	PALSAR Texture measure energy extracted from May HV back-scattering with a window size of 3x3	0.36
QMCH	LVIS Canopy height profile was calculated from canopy reflection in the waveform, ground-canopy ratio was 2	0.35
Trailing Edge	LVIS Height difference between first signal larger than half of the maximum intensity and the signal end	0.32
Tex_Jun_CON_HV_Win3	PALSAR Texture measure contrast extracted from June HV back- scattering with a window size of 3x3	0.31
Tex_Jun_CON_HV_Win15	PALSAR Texture measure contrast extracted from June HV back- scattering with a window size of 15x15	0.31

Table 2 (Continued from preceding page) - Variable relative importance for deciduous plots.

Tex_Jun_DIS_HV_Win15	PALSAR Texture measure dissimilarity extracted from June HV backscattering with a window size of 15x15	0.26
Tex_May_COR_HV_Win3	PALSAR Texture measure correlation extracted from May HV backscattering with a window size of 3x3	0.23
Tex_Nov_DIS_HV_Win3	PALSAR Texture measure dissimilarity extracted from November HV backscattering with a window size of 3x3	0.21
Tex_Nov_ENE_HH_Win3	PALSAR Texture measure energy extracted from November HH backscattering with a window size of 3x3	0.16
HMRatio	LVIS Ratio between the maximum height and Height Of Median Energy (HOME)	0.15
Tex_Aug_CON_HV_Win15	PALSAR Texture measure contrast extracted from August HV back-scattering with a window size of 15x15	0.12
Tex_Nov_ENT_HH_Win3	PALSAR Texture measure entropy extracted from November HH backscattering with a window size of 3x3	0.12
Tex_Jun_DIS_HV_Win3	PALSAR Texture measure dissimilarity extracted from June HV backscattering with a window size of 3x3	0.09
Tex_Jun_COR_HV_Win3	PALSAR Texture measure correlation extracted from June HV backscattering with a window size of 3x3	0.09
Tex_May_HOM_HV_Win15	PALSAR Texture measure homogeneity extracted from May HV backscattering with a window size of 15x15	0.07
Tex_May_DIS_HV_Win15	PALSAR Texture measure dissimilarity extracted from May HV backscattering with a window size of 15x15	0.06
Tex_May_HOM_HH_Win15	PALSAR Texture measure homogeneity extracted from May HH backscattering with a window size of 15x15	0.06

Acknowledgements

This work was supported through NASA's Biodiversity Program under grant number NNX-09AK16G and a Graduate Assistantship from the State University of New York College of Environmental Science and Forestry.

References

Attarchi S., Gloaguen R. (2014) - Improving the Estimation of Above Ground Biomass Using Dual Polarimetric PALSAR and ETM+ Data in the Hyrcanian Mountain Forest (Iran). Remote Sensing, 6: 3693-3715. doi: http://dx.doi.org/10.3390/rs6053693.

Avitabile V., Baccini A., Friedl M.A., Schmullius C. (2012) - Capabilities and limitations of Landsat and land cover data for aboveground woody biomass estimation of Uganda. Remote Sensing of Environment, 117: 366-380. doi: http://dx.doi.org/10.1016/j.

- rse.2011.10.012.
- Banskota A., Wynne R.H., Johnson P., Emessiene B. (2009) Synergistic use of very high-frequency radar and discrete-LiDAR return for estimating biomass in temperate hardwood and mixed forests. Proceedings Silvilaser, College Station, Texas, USA, pp. 81-87.
- Carreiras J.M., Vasconcelos M.J., Lucas R.M. (2012) *Understanding the relationship between aboveground biomass and ALOS PALSAR data in the forests of Guinea-Bissau* (*West Africa*). Remote Sensing of Environment, 121: 426-442. doi: http://dx.doi.org/10.1016/j.rse.2012.02.012.
- Chang A., Jung J., Kim Y. (2015) Estimation of forest stand diameter class using airborne lidar and field data. Remote Sensing Letters, 6 (6): 419-428. doi: http://dx.doi.org/10.1 080/2150704X.2015.1035770.
- Dees M., Straub C., Langar P., Koch B. (2006) Remote sensing based concepts utilizing SPOT5 and for forest habitat mapping and monitoring under the EU Habitat Directive. ONP 10 Test & Benchmarks Report, Part of the geoland project reporting dossier, pp. 53-78.
- Dees M., Koch B. (2008) Forestry applications. Advances in Photogrammetry. Remote Sensing and Spatial Information Sciences, 2008 ISPRS Congress Book, pp. 439-468.
- Deng S., Katoh M., Guan Q., Yin N., Li M. (2014) Estimating Forest Aboveground Biomass by Combining ALOS PALSAR and WorldView-2 Data: A Case Study at Purple Mountain National Park, Nanjing, China. Remote Sensing, 6: 7878-7910. doi: http://dx.doi.org/10.3390/rs6097878.
- Dobson M.C., Ulaby F.T., Le Toan T., Beaudion A., Kaschischke E.S., Christensen N. (1992) *Dependence of radar backscatter on coniferous forest biomass*. IEEE Transactions on Geoscience and Remote Sensing, 30 (2): 412-415. doi: http://dx.doi.org/10.1109/36.134090.
- Dube T., Mutanga O. (2015) Evaluating the utility of the medium-spatial resolution Landsat 8 multispectral sensor in quantifying aboveground biomass in uMgeni catchment, South Africa. ISPRS Journal of Photogrammetry and Remote Sensing, 101: 36-46. doi: http://dx.doi.org/10.1016/j.isprsjprs.2014.11.001.
- Fassnacht F.E., Hartig F., Latifi H., Berger C., Hernández J. (2014) *Importance of sample size, data type and prediction method for remote sensing-based estimations of aboveground forest biomass*. Remote Sensing of Environment, 154: 102-114. doi: http://dx.doi.org/10.1016/j.rse.2014.07.028.
- Filippi A.M., Güneralp I., Randall J. (2014) Hyperspectral remote sensing of aboveground biomass on a river meander bend using multivariate adaptive regression splines and stochastic gradient boosting. Remote Sensing Letters, 5 (5): 432-441. doi: http://dx.doi.org/10.1080/2150704X.2014.915070.
- Hamdan O., Aziz H.K., Rahman K.A. (2011) Remotely sensed L-band SAR data for tropical forest biomass estimation. Journal of Tropical Forest Science, 23 (3): 318-327.
- Hamdan O., Khali Aziz H., Mohd Hasmadi I. (2014) *L-band ALOS PALSAR for biomass estimation of Matang Mangroves, Malaysia*. Remote Sensing of Environment, 155: 69-78. doi: http://dx.doi.org/10.1016/j.rse.2014.04.029.
- Huang W., Sun G., Dubayah R., Cook B., Montesano P., Ni W., Zhang Z. (2013) Mapping biomass change after forest disturbance: Applying LiDAR footprint-derived models

- at key map scales. Remote Sensing of Environment, 134: 319-332. doi: http://dx.doi.org/10.1016/j.rse.2013.03.017.
- Hyyppä J., Hyyppä H., Yu X., Kaartinen H., Kukko A., Holopainen M. (2009) Forest inventory using small-footprint airborne LiDAR. Forest Inventory Using Small Footprint Airborne Topographic Laser Ranging and Scanning Principles. CRC Press, Boca Raton, pp. 335-370.
- Jin H., Mountrakis G., Stehman (2014) Assessing integration of intensity, polarimetric scattering, interferometric coherence and spatial texture metrics in PALSAR-derived land cover classification. ISPRS Journal of Photogrammetry and Remote Sensing, 98: 70-84. doi: http://dx.doi.org/10.1016/j.isprsjprs.2014.09.017.
- Koch B. (2010) Status and future of laser scanning, synthetic aperture radar and hyperspectral remote sensing data for forest biomass assessment. ISPRS Journal of Photogrammetry and Remote Sensing, 65 (6): 581-590. doi: http://dx.doi.org/10.1016/j.isprsjprs.2010.09.001.
- Liaw A., Wiener M. (2002) Classification and Regression by Random Forest. R News, 2 (3): 18-22.
- Lu D. (2005) Aboveground biomass estimation using Landsat TM data in the Brazilian Amazon. International Journal of Remote Sensing, 26 (12): 2509-2525. doi: http://dx.doi.org/10.1080/01431160500142145.
- Lu D. (2006) *The potential and challenge of remote sensing-based biomass estimation*. International Journal of Remote Sensing, 27 (7): 1297-1328. doi: http://dx.doi.org/10.1080/01431160500486732.
- Lu D., Chen Q., Wang G., Liu L., Li G., Moran E. (2014) A survey of remote sensing-based aboveground biomass estimation methods in forest ecosystems. International Journal of Digital Earth, 9 (1): 63-105. doi: http://dx.doi.org/10.1080/17538947.2014.990526.
- Mallet C., Bretar F. (2009) *Full waveform topographic LiDAR: State-of-the-art*. ISPRS Journal of Photogrammetry and Remote Sensing, 64 (1): 1-16. doi: http://dx.doi.org/10.1016/j.isprsjprs.2008.09.007.
- Maltamo M., Malinen J., Packalén P., Suvanto A., Kangas J. (2006) *Nonparametric estimation of stem volume using airborne laser scanning, aerial photography and stand register data*. Canadian Journal of Forest Research, 36 (2): 426-436. doi: http://dx.doi.org/10.1139/x05-246.
- Masato H., Saigusa N., Yamagata Y., Hirano T. (2015) *Regional forest biomass estimation using ICESat/GLAS spaceborn LiDAR over Borneo*. Carbon Management, 6 (1-2): 19-33. doi: http://dx.doi.org/10.1080/17583004.2015.1066638.
- Mitchard E.T.A., Saatchi S.S., White L.J.T., Abernethy K.A., Jeffery K.J., Lewis S.L., Collins M., Lefsky M.A., Leal M.E., Woodhouse I.H., Meir P. (2012) Mapping tropical forest biomass with radar and spaceborne LiDAR in Lope National Park, Gabon: Overcoming problems of high biomass and persistent cloud. Biogeosciences, 9: 179-191. doi: http://dx.doi.org/10.5194/bg-9-179-2012.
- Moghaddam M., Dungan J.L., Acker S. (2002) Forest variable estimation from fusion of SAR and multispectral optical data. IEEE Transactions on Geoscience and Remote Sensing, 40 (10): 2176-2187. doi: http://dx.doi.org/10.1109/TGRS.2002.804725.
- Morel A.C., Saatchi S.S., Malhi Y., Berry N.J., Banin L., Burslem D., Nilus R., Ong R.C. (2011) Estimating aboveground biomass in forest and oil palm plantation in Sabah,

- - *Malaysian Borneo using ALOS PALSAR data*. Forest Ecology and Management, 262 (9): 1786-1798. doi: http://dx.doi.org/10.1016/j.foreco.2011.07.008.
- Mui-How P., Saito H. (2003) Estimation of biomass of a mountainous tropical forest using Landsat TM data. Canadian Journal of Remote Sensing, 29 (4): 429-440. doi: http://dx.doi.org/10.5589/m03-005.
- Peregon A., Yamagata Y. (2013) *The use of ALOS/PALSAR backscatter to estimate above-ground forest biomass: A case study in Western Siberia*. Remote Sensing of Environment, 137: 139-146. doi: http://dx.doi.org/10.1016/j.rse.2013.06.012.
- Rignot E., Salas W.A., Skole D.A. (1997) Mapping deforestation and secondary growth in Rondia Brazil, using imaging radar and thematic mapper data. Remote Sensing of Environment, 59 (2): 167-179. doi: http://dx.doi.org/10.1016/S0034-4257(96)00150-2.
- Santoro M., Askne J., Smith G., Fransson J.E.S. (2002a) *Stem volume retrieval in boreal forests from ERS-1/2 interferometry*. Remote Sensing of Environment, 81 (1): 19-35. doi: http://dx.doi.org/10.1016/S0034-4257(01)00329-7.
- Santoro M., Schmullius C., Eriksson L., Hese S. (2002b) *The Siberia and Siberia-II* projects: an overview. Proceedings of SPIE, SPIE Conference Crete, 4886: 247-256.
- Ranson K.J., Sun G. (1994) *Mapping biomass of northern forests using multifrequency SAR data*. IEEE Transactions on Geoscience and Remote Sensing, 32 (5): 1117-1124. doi: http://dx.doi.org/10.1109/36.295053.
- Sarker M., Nichol J., Ahmad B., Busu I., Rahman A. (2012) Potential of texture measurements of two-date dual polarization PALSAR data for the improvement of forest biomass estimation. ISPRS Journal of Photogrammetry and Remote Sensing, 69: 146-166. doi: http://dx.doi.org/10.1016/j.isprsjprs.2012.03.002.
- Straub C., Dees M., Weinacker H., Koch B. (2009) *Using airborne laser scanner data and CIR orthophotos to estimate the stem volume of forest stands*. Photogrammetrie, Fernerkundung, Geoinformation, 30 (3): 277-287. doi: http://dx.doi.org/10.1127/0935-1221/2009/0022.
- Sun G., Ranson K.J., Guo Z., Zhang Z., Montesano P., Kimes D. (2011) *Forest biomass mapping from lidar and radar synergies*. Remote Sensing of Environment, 115: 2906-2916. doi: http://dx.doi.org/10.1016/j.rse.2011.03.021.
- Suzuki R., Kim Y., Ishii R. (2013) Sensitivity of the backscatter intensity of ALOS/PALSAR to the above-ground biomass and other biophysical parameters of boreal forest in Alaska. Polar Science, 7 (2): 100-112. doi: http://dx.doi.org/10.1016/j.polar.2013.03.001.
- Swatantran A., Dubayah R., Roberts D., Hofton M., Bryan Blair J. (2011) *Mapping biomass and stress in the Sierra Nevada using lidar and hyperspectral data fusion*. Remote Sensing of Environment, 115: 2917-2930. doi: http://dx.doi.org/10.1016/j.rse.2010.08.027.
- Tang H., Brolly M., Zhao F., Strahler A.H., Schaaf C.L., Ganguly S., Zhang G., Dubayah R. (2014) Deriving and validating Leaf Area Index (LAI) at multiple spatial scales through lidar remote sensing: A case study in Sierra National Forest, CA. Remote Sensing of Environment, 143: 131-141. doi: http://dx.doi.org/10.1016/j.rse.2013.12.007.
- Thiel C., Drezet P., Weise C., Quegan S., Schmullius C. (2006) *Radar remote sensing for the delineation of forest cover maps and the detection of deforestation*. Forestry, 79 (5): 589-597. doi: http://dx.doi.org/10.1093/forestry/cpl036.
- Yanjun S., Guo Q., Xue B., Hu T., Alvarez O. (2016) Spatial distribution of forest

- aboveground biomass in China: Estimation through combination of spaceborne lidar, optical imagery, and forest inventory data. Remote Sensing of Environment, 173:187-199. doi: http://dx.doi.org/10.1016/j.rse.2015.12.002.
- Zhuang W., Mountrakis G. (2014a) An accurate and computationally efficient algorithm for ground peak identification in large footprint waveform LiDAR data. ISPRS Journal of Photogrammetry and Remote Sensing, 95: 81-92. doi: http://dx.doi.org/10.1016/j. isprsjprs.2014.06.004.
- Zhuang W., Mountrakis G. (2014b) *Ground peak identification in dense shrub areas using large footprint waveform LiDAR and Landsat images*. International Journal of Digital Earth, 8 (10): 805-824. doi: http://dx.doi.org/10.1080/17538947.2014.942716.
- Zhuang W., Mountrakis G., Wiley Jr. J., Beier C. (2015) Estimation of Aboveground Forest Biomass Using Metrics Based on Gaussian Decomposition of Waveform Lidar Data. International Journal of Remote Sensing, 36 (7): 1871-1889. doi: http://dx.doi.org/10.1080/01431161.2015.1029095.
- © 2016 by the authors; licensee Italian Society of Remote Sensing (AIT). This article is an open access article distributed under the terms and conditions of the Creative Commons Attribution license (http://creativecommons.org/licenses/by/4.0/).